**Proceedings of the INMM & ESARDA Joint Annual Meeting**
**May 22-26, 2023**

# Fireball Chemistry and Hydrodynamics of Laser Ablation Plasmas

**Emily H. Kwapis[1], Jacob W. Posey[2], Enrique Medici[1], Kira Berg[3], Ryan W. Houim[2], and Kyle C. Hartig[1]**

[1]Nuclear Engineering Program, Herbert Wertheim College of Engineering, University of Florida, Gainesville, Florida 32611, USA

[2]Department of Mechanical and Aerospace Engineering, Herbert Wertheim College of Engineering, University of Florida, Gainesville, Florida 32611, USA

[3]Department of Agricultural and Biological Engineering, Herbert Wertheim College of Engineering, University of Florida, Gainesville, Florida 32611, USA

## ABSTRACT

Developing measurement technologies to monitor nuclear-relevant materials in the environment aims to prevent the proliferation of nuclear weapons by detecting undeclared nuclear fuel cycle activities. Standoff, field-deployable optical detection systems based on laser spectroscopy offer the capability to measure spectrochemical signatures without sample preparation by exciting a target material via laser ablation followed by diagnostics to detect photons emitted from the ensuing laser-produced plasma. Spectroscopic signatures are dependent on plasma conditions, where the spatial and physicochemical properties of the plasma change rapidly with time and are highly sensitive to both experimental and environmental conditions. Uranium and plutonium plasmas react readily with oxygen in the atmosphere, leading to the formation of molecular species and considerably influencing signature interpretation. This work aims to address the complex plasma plume hydrodynamics and mixing processes with the surrounding atmosphere to explain the high-temperature gas-phase oxidation reactions and kinetics of laser ablation plasmas. Experimental measurements are presented alongside high-fidelity multi-physics simulations, providing visualizations of the expansion dynamics and thermochemical plume dynamics. Gas-phase molecular species are observed to form in the thin plume periphery within the first few nanoseconds of the simulation in the presence of large temperature gradients (thousands of Kelvin) and strong shockwaves. Intermixing between reacting plasma-gas species is shown to be driven by diffusion and hydrodynamic processes such as vortex formation, while shockwaves are observed to pre-heat the air ahead of the plasma plume yet otherwise remain uninvolved in plasma plume chemistry.

## INTRODUCTION

Analytical chemistry methods in laser spectroscopy offer in-field measurement capabilities requiring no sample preparation to detect and characterize nuclear-relevant materials at standoff distances. Through the process of pulsed laser ablation (LA), a high-powered pulsed laser is used to ionize and excite a target material to create a luminous micro-plasma that emits photons at discrete energies as it de-excites. These characteristic photons are collected and binned, generating an optical spectrum to fingerprint the elemental and isotopic composition of the vaporized sample.

The characterization of signatures in the optical spectrum is determined by the complex and transient conditions of the laser ablation plasma, where the plasma response is highly sensitive to laser parameters and atmospheric conditions. Metal and actinide LA plasmas readily react with oxygen in the surrounding environment to form simple gas-phase oxides that alter the composition of the plasma plume while introducing molecular signatures to the optical spectrum that overlap with and obscure electronic transitions associated with atomic and ionic species. Furthermore, the concentration of oxygen present in the system has been shown to alter reaction pathways and kinetics [1-2], further complicating the spectroscopic analysis.

Chemical reactions in laser ablation plasmas are driven by favorable thermodynamics and intermixing between reactive plasma and ambient gas species. Immediately after laser ablation, the plasma plume is dominated by atomic and ionic species while temperatures are measured to be greater than 10,000 K [3-5]. The formation of molecular species is generally favored at lower temperatures (<6,000 K) [6-7] and is experimentally measured at later times ($\geq$2 μs) in the plasma evolution [8-10]. Molecules with higher dissociation energies ($D_0$ > 6 eV) can form at higher temperatures and earlier times, while those with lower dissociation energies preferably form in the periphery of the plasma plume where temperatures are lower [11-12]. Experimental and computational measurements indicate that spatial distributions of chemical species in the plasma plume and intermixing between plasma-gas species are primarily driven by diffusion processes and large concentration gradients along the periphery of the plasma plume [9, 13-15], which parallels hydrodynamical processes characterizing non-premixed diffusion flames [16-17]. Another publication suggests that laser-induced shockwaves impact plasma plume chemistry as well, stating that LA shockwave dynamics works to prevent mixing between the plasma plume and ambient atmosphere [18], thereby impeding the formation of molecular species in the plume until the shockwave weakens and transitions to an acoustic wave. In contrast, computational modeling on plume hydrodynamics and chemistry does not currently support this hypothesis [13].

This work aims to elucidate the impact of plume hydrodynamics on LA plasma chemistry. Experimental measurements and computational modeling will be provided to explain the universal mixing processes between plasma and ambient gas species that influence the spatiotemporal evolution of chemical species in the plasma plume and alter spectroscopic signatures. Opposing viewpoints that currently exist in the literature on the involvement of shockwaves in plasma plume chemistry will also be addressed.

## EXPERIMENTAL AND COMPUTATIONAL METHODS

Experimental Setup

Ns-LA is performed on an aluminum sputtering target (MSE Supplies, 99.9% purity) using the fundamental wavelength (1064 nm) of a Q-switched Nd:YAG laser (Continuum Surelite II-10). The energy of the laser beam is set to 25.0±0.2 mJ, and a 100 mm focal length plano-convex lens is used to focus the beam onto the target to produce a 500 μm diameter crater. To perform focused shadowgraphy, a second Nd:YAG laser is frequency-doubled to a wavelength of 532 nm and is used to excite a dilute Rhodamine 6G methanol solution. Upon excitation by the laser light the dye undergoes fluorescence and serves as an incoherent illumination source to backlight the shadowgraphic images. Shadowgraphs are focused onto the sensor of an emICCD camera (Princeton Instruments PI-MAX4) using a 150 mm focal length plano-convex lens, while a fluorescence filter is also placed after the lens to reduce light exposure to the camera.

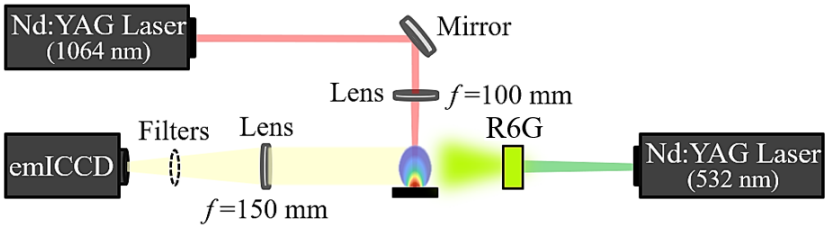


**Figure 1. Focused shadowgraph experimental setup.**

Computational Modeling

The reactive multi-phase flow code HyBurn is applied to model the chemical dynamics of laser ablation aluminum plasmas. 2D axisymmetric Eulerian simulations are defined on a square mesh (8 mm x 8 mm) with a resolution of 5 µm and rotational symmetry about the y-axis (see Fig. 2). The plasma plume is initialized post-LA as a homogeneous aluminum fireball with circular geometry and a radius of 250 µm. The initial temperature and pressure of the plume are set to 20,000 K and 70 MPa, respectively, where these values were selected based on experimental measurements. The plume is placed within a 500 µm diameter crater with a depth of 50 µm, and the background gas surrounding the plume is defined as air at standard temperature and pressure. Aluminum combustion chemistry and related post-detonation phenomena including the dissociation of air are implemented using thermodynamic properties pulled from NASA polynomials [19-20], Lennard-Jones transport parameters [21], and reported reaction mechanisms and rate constants [21-22]. Post-detonation chemical phenomena for uranium and plutonium LA plasmas are unable to be modeled due to the lack of data on these required gas-phase parameters. Real gas effects are modeled using the Becker-Kistiakowsky-Wilson (BKW) equation of state (EoS), while diffusion processes are included as well.

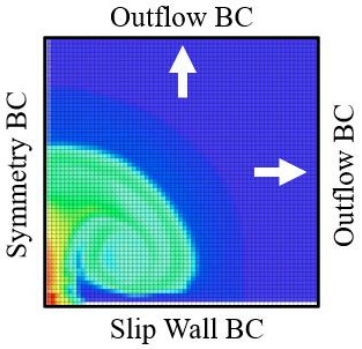


**Figure 2. Computational setup for the 2D axisymmetric simulation of the Al plume.**

Simulations are run on a cluster of the University of Florida supercomputer HiperGator using 50 processors, where runtimes averaged around 12 hours for the models generated in this work. Data is post-processed and analyzed using in-house Python algorithms in addition to the open-source visualization and graphical analysis software VisIt.

## RESULTS AND DISCUSSION

Experimental Measurements of Shockwave Dynamics.

The propagation and attenuation of the external laser-induced shockwave generated during LA is studied in this work to determine parameter values towards the initialization of the computational model. Focused shadowgraphy is performed to image the radially expanding hemispherical shock over time, providing time-resolved measurements of the shock front radius. A semi-empirical curve based on a power law dependence is then fitted to the shock expansion trajectory, and a propagation velocity of 8250±180 m/s is determined from the derivative of this curve at a time delay of 15 ns. Using the propagation velocity of the shockwave as an input into the gas-dynamics

equations, the thermodynamic properties of the shock-heated flow immediately behind the shock front can also be determined. The Rankine-Hugoniot relations for an inert shock with variable specific heat are solved numerically in this work to provide temperature and pressure values of 20,800±800 K and 73.5±3.3 MPa at 15 ns, respectively. The maximum temperature that can be modeled by the multi-physics code is 20,000 K, hence, the initial simulation temperature is set to this value while the initial pressure is set to 70 MPa. Furthermore, the geometry and dimensions of the initial plume and shockwave in the computational model are initialized as circular with a radius of 250 µm based on the shadowgraphic measurements. However, it should be acknowledged that the plasma plume is detached from and located behind the laser-induced shockwave in experimental measurements.

A comparison between the shockwave dynamics and associated properties between the experimental measurements and computational model is shown in Fig. 3. For the first 300 ns, the propagation velocity of the laser-induced shockwave is experimentally measured to be greater than the predicted velocity in the simulation. This indicates the expansion velocity of the shockwave in the simulation is underestimated at early times and overestimated at later times, although values do remain comparable over the entire simulation. Both experimentally-measured and simulated shockwaves transition to an acoustic wave at times later than 5 µs when the shocks decelerate to velocities lower than the speed of sound in air (343 m/s). The acoustic wave is still visible in the shadowgraphic images out to a time delay of 10 µs, beyond which the radius of the wave is larger than the field of view of the camera (see Fig. 4). Keeping with the comparable propagation velocities, the simulated pressure and temperature of the shock-heated air are also observed to be in agreement with the experimental values determined using the Rankine-Hugoniot relations for the first 5 µs of the shockwave propagation. Thermodynamic properties are not compared for later times because the Hugoniot analysis implemented is only valid for shockwaves and is not applicable to acoustic waves.

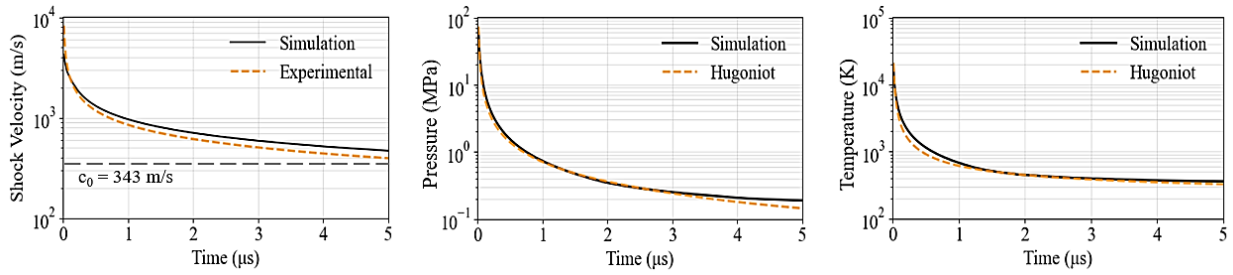


**Figure 3. Comparison of the experimental and computational shockwave propagation and shock-heated air properties. The Hugoniot curves are determined using experimental data.**

Beyond the radially expanding shockwave, Figure 4 also provides a visual comparison of other fronts in the system that alter the density of the gas-dynamic flow. Shadowgraphs show the presence of a hemispherical ionization front located behind the shock front for time delays ≤1 µs, where an ionization front marks the boundary between shock-heated and ionized gas and is located ahead of the plasma plume [23]. Schlieren images produced by the computational model also display a smaller hemispherical feature behind the shock front with comparable dimensions to the measured ionization front. However, ionization processes are not currently captured by the computational model, eliminating the possibility of an ionization front in the simulation. Instead, the hemisphere marks the dissociation of air and formation of nitric oxide (NO) in the Schlieren

images. The plume periphery is consistently located approximately 50 μm behind the NO front throughout the simulation. The periphery of the plasma plume itself first becomes resolvable in the measured shadowgraphic images around 10 μs, where the relatively hemispherical plume is observed to lengthen in the direction perpendicular to the sample surface. This axial length is observed to be larger in the simulated images, although the overall plume shapes do remain comparable. Possible reasons for this disagreement include the absence of ionization and radiative processes in the computational model, as well as assumptions involved in defining the initial mass and energy of the fireball.

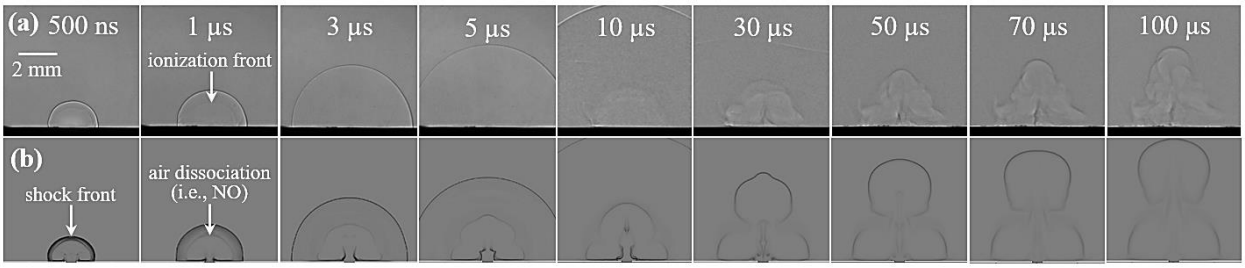


**Figure 4. Comparison of (a) shadowgraphic measurements of the laser-induced shockwave and Al plasma to (b) simulated Schlieren images.**

Multiphase Thermochemical Plume Dynamics.

Reactive laser ablation plasmas are governed by a complex interplay between hydrodynamic intermixing between plasma and ambient gas species, high-temperature thermodynamics, and rapid chemical reactions. Atomic plume species readily react with oxygen in the atmosphere to form simple gas-phase molecules, which condense into nanoparticles and nanoclusters over several milliseconds as the plasma cools [24-26]. The first 100 μs of the evolving plume composition is modeled in this work, encompassing a homogeneous Al (g) plume at the initial time step to a plume predominantly consisting of $Al_2O_3$ (l) at late times.

Within the first few nanoseconds of the simulation, the formation of several gas-phase oxides including AlO, $AlO_2$, $Al_2O$, and $Al_2O_2$ is observed in small quantities in the thin periphery of the vapor plume. The formation of these oxide species indicates the diffusion of oxygen into the aluminum plume to form a thin chemical reaction zone. Over this spatial region, large concentration and thermal gradients are present, marking the transition region between the hot plume core (20,000 K) and ambient atmosphere (300 K). A supersonic shockwave separates from the vapor plume, forming a region of shock-heated air between the plume and shock that is characterized by a temperature of a few thousand Kelvin. The formation of the condensation product $Al_2O_3$ (l) is first observed along the sample surface around 30 ns. These results indicate that molecular species form in LA plasma plumes at very earlier times when spectroscopic methods are unable to experimentally measure the chemical composition of the plume due to large sources of continuum radiation. Strong shockwaves exist over this timescale, and are not observed to prevent intermixing between plasma-gas species or impede chemical species formation.

During the first few microseconds of the simulation, the vapor plume rapidly expands outwards and interacts with the edges of the crater to form a mushroom-shaped cloud. AlO (g) is pulled up into the vortices of the mushroom cloud to react with Al (g) to form $Al_2O$ (g) (see 0.5 μs in Fig.

5) while several other molecular species and oxygen (both O and $O_2$) are pulled up through the stem of the fireball (see 5 µs in Fig. 5). As the vapor plume expands outwards in the direction perpendicular to the sample, a second set of vortices forms near the sample surface (see 15 µs in Fig. 5). The simulation indicates that the main constituent of this lower half of the vapor plume is liquid-phase aluminum oxide, $Al_2O_3$ (l), while the gas-phase species tend to predominate the head of the fireball till around 30 µs and later. For these later time delays, $Al_2O_3$ (l) is observed to dominate the composition of the fireball while only small quantities of Al (g), AlO (g), and $Al_2O$ (g) remain.

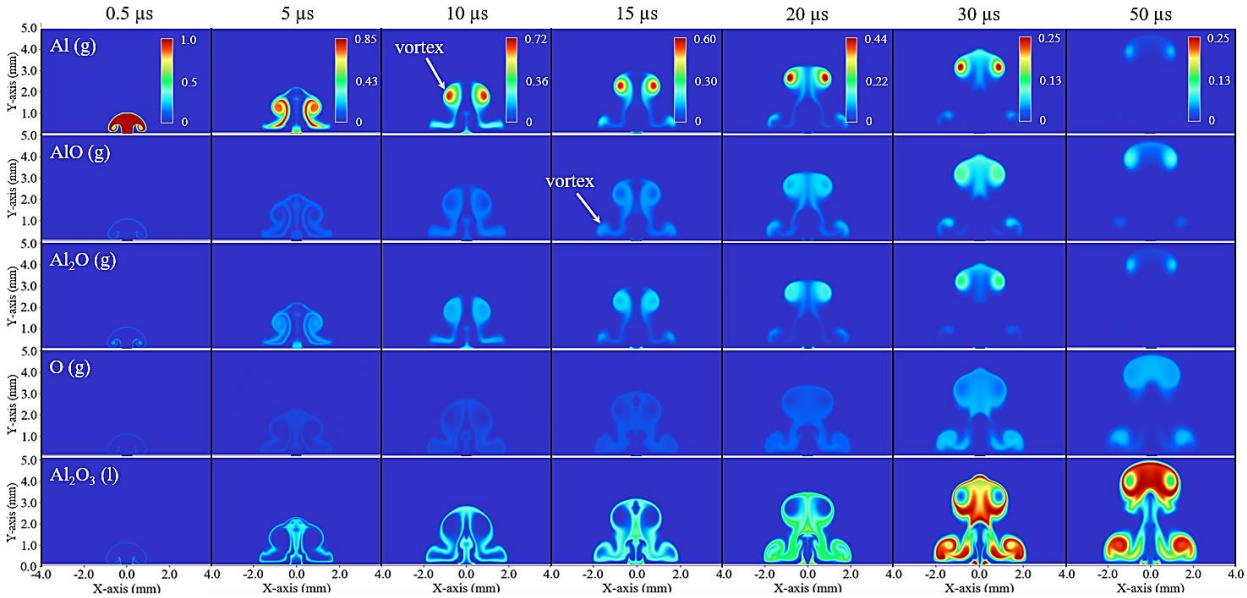


**Figure 5. Selected mass fractions demonstrating the spatiotemporal evolution of chemical species in the aluminum plume. Colormaps are scaled by column.**

## CONCLUSION

The shock physics and chemical dynamics of laser ablation aluminum plasmas have been investigated to explain the impact of physical processes on post-detonation plume chemistry. Focused shadowgraphy was performed to experimentally measure the propagation of laser-induced shockwaves through air and to image the aluminum plasma plume at late times (≥10 µs). Measurements of the shockwave were combined with the Rankine-Hugoniot relations to provide estimates on initial conditions for a computational multi-physics model of the expanding fireball. Simulated results demonstrated the spatiotemporal evolution of chemical species in the aluminum vapor plume, showing the formation of both gas-phase and liquid-phase aluminum oxides in the plume periphery for times as early as 30 ns. Diffusion and hydrodynamic processes including vortex formation were shown to encourage intermixing between reacting plasma-gas species while strong shockwaves were shown to be largely uninvolved in these mixing processes.

## ACKNOWLEDGMENTS

The authors would like to acknowledge funding support from the National Nuclear Security Administration Consortium for Monitoring, Technology, and Verification (DE-NA0003920), National Science Foundation (CHE19105301), and Defense Threat Reduction Agency Interaction of Ionizing Radiation with Matter University Research Alliance (HDTRA1-20-2-0002, HDTRA1-19-1-0025).

## REFERENCES

[1] M.A. Burton, A.W. Auner, J.C. Crowhurst, P.S. Boone, L.A. Finney, D.G. Weisz, B. Koroglu, I. Jovanovic, H.B. Radousky, and K.B. Knight. The effect of oxygen concentration on the speciation of laser ablated uranium, *Sci. Rep.* 12, 4030 (2022).

[2] M.T. Butterfield, T. Durakiewicz, E. Guziewicz, J.J. Joyce, A.J. Arko, K.S. Graham, D.P. Moore, and L.A. Morales. Photoemission of surface oxides and hydrides of delta plutonium, *Surf. Sci.* 571(1-3), 74-82 (2004).

[3] S.S. Harilal, C.V. Bindhu, R.C. Issac, V.P.N. Nampoori, and C.P.G. Vallabhan. Electron density and temperature measurements in a laser produced carbon plasma, *J. Appl. Phys.* 82(5), 2140-2146 (1997).

[4] K. Muraoka and A. Kono. Laser Thomson scattering for low-temperature plasmas, *J. Phys. D: Appl. Phys.* 44(4), 043001 (2011).

[5] K.K. Herrera, E. Tognoni, N. Omenetto, B.W. Smith, and J.D. Winefordner. Semi-quantitative analysis of metal alloys, brass and soil samples by calibration-free laser-induced breakdown spectroscopy: Recent results and considerations, *J. Anal. At. Spectrom.* 24(4), 413-425 (2009).

[6] K.C. Hartig, B.E. Brumfield, M.C. Phillips, and S.S. Harilal. Impact of oxygen chemistry on the emission and fluorescence spectroscopy of laser ablation plumes, *Spectrochim. Acta Part B: At. Spectrosc.* 135, 54-62 (2017).

[7] P.J. Skrodzki, M. Burger, I. Jovanovic, M.C. Phillips, J. Yeak, B.E. Brumfield, and S.S. Harilal. Plume dynamics and gas-phase molecular formation in transient laser-produced uranium plasmas, *Phys. Plasmas* 26(8), 083508 (2019).

[8] C. Kimblin, R. Trainham, G.A. Capelle, X. Mao, and R.E. Russo. Characterization of laser-induced plasmas as a complement to high-explosive large-scale detonations, *AIP Adv.* 7(9), 095208 (2017).

[9] E.R. Wainwright, S.W. Dean, F.C. De Lucia Jr., T.P. Weihs, and J.L. Gottfried. Effect of sample morphology on the spectral and spatiotemporal characteristics of laser-induced plasmas from aluminum, *Appl. Phys. A* 126, 83 (2020).

[10] E.H. Kwapis, E. Villa-Aleman, and K.C. Hartig. Spectroscopic signatures and oxidation characteristics of nanosecond laser-induced cerium plasmas, *Spectrochim. Acta Part B: At. Spectrosc.* 200, 106610 (2023).

[11] A. De Giacomo and J. Hermann. Laser-induced plasma emission: From atomic to molecular spectra, *J. Phys. D: Appl. Phys.* 50, 183002 (2017).

[12] D.G. Weisz, J.C. Crowhurst, M.S. Finko, T.P. Rose, B. Koroglu, R. Trappitsch, H.B. Radousky, W.J. Siekhaus, M.R. Armstrong, B.H. Isselhardt, M. Azer, and D. Curreli. Effects of plume hydrodynamics and oxidation on the composition of a condensing laser-induced plasma, *J. Phys. Chem. A* 122(6), 1584-1591 (2018).

[13] S.V. Shabanov and I.B. Gornushkin. Modeling chemical reactions in laser-induced plasmas, *Appl. Phys. A* 121, 1087-1107 (2015).

[14] J. Hermann, A. Lorusso, A. Perrone, F. Strafella, C. Dutouquet, and B. Torralba. Simulation of emission spectra from nonuniform reactive laser-induced plasmas, *Phys. Rev. E* 92(5), 053103 (2015).
[15] T.E. Itina, J. Hermann, P. Delaporte, and M. Sentis. Laser-generated plasma plume expansion: Combined continuous-microscopic modeling, *Phys. Rev. E* 66(6 Pt 2), 066406 (2002).
[16] I. Glassman and R.A. Yetter. *Combustion*, Chapter 6: Diffusion Flames, 4th Ed. Elsevier Inc., pp. 311-377 (2008).
[17] F. Dietzsch, A. Scholtissek, F. Hunger, and C. Hasse. Impact of thermal diffusion on the structure of non-premixed flames, *Combust. Flame* 194, 352-362 (2018).
[18] S.S. Harilal, B.E. Brumfield, B.D. Cannon, and M.C. Phillips. Shock wave mediated plume chemistry for molecular formation in laser ablation plasmas, *Anal. Chem.* 88(4), 2296-2302 (2016).
[19] M.W. Chase Jr., C. Davies, J.R. Downey Jr., D. Frurip, R. McDonald, and A. Syverud. *JANAF Thermochemical Tables*, 3rd Ed., Pts. 1 & 2, *JPCRD* 14, (1985).
[20] B. McBride, S. Gordon, and M. Reno. Coefficients for calculating thermodynamic and transport properties of individual species, NASA Technical Memorandum 4513, (1993).
[21] A.M. Starik, P.S. Kuleshov, A.S. Sharipov, N.S. Itiova, and C. Tsai. Numerical analysis of nanoaluminum combustion in steam, *Combust. Flame* 161, 1659-1667 (2014).
[22] C. Johnston and A. Brandis. Modeling of nonequilibrium CO Fourth-Positive and CN Violet emission in $CO_2$-$N_2$ gases, *JQSRT* 149, 303-317 (2014).
[23] G. Callies, P. Berger, and H. Hugel. Time-resolved observation of gas-dynamic discontinuities arising during excimer laser ablation and their interpretation, *J. Phys. D: Appl. Phys.* 28(4), 794-806 (1995).
[24] R.E. Russo, X. Mao, J.J. Gonzalez, V. Zorba, and J. Yoo. Laser ablation in analytical chemistry, *Anal. Chem.* 85, 6162-6177 (2013).
[25] M. Kim, S. Osone, T. Kim, H. Higashi, and T. Seto. Synthesis of nanoparticles by laser ablation: A review, *KONA Powder Part. J.* 34, 80-90 (2017).
[26] M.S. Tillack, D.W. Blair, and S.S. Harilal. The effect of ionization on cluster formation in laser ablation plumes, *Nanotechnology* 15(3), 390-403 (2004).